journal

J. Am. Ceram. Soc., **81** [11] 2831–40 (1998)

Microstructural Design of Silicon Nitride with Improved Fracture Toughness: II, Effects of Yttria and Alumina Additives

Ellen Y. Sun,* Paul F. Becher,* Kevin P. Plucknett,*,† Chun-Hway Hsueh,* Kathleen B. Alexander,* and Shirley B. Waters

Metals and Ceramics Division, Oak Ridge National Laboratory, Oak Ridge, Tennessee 37831-6068

Kiyoshi Hirao* and Manuel E. Brito*

National Industrial Research Institute of Nagoya, Nagoya, Japan

Significant improvements in the fracture resistance of self-reinforced silicon nitride ceramics have been obtained by tailoring the chemistry of the intergranular amorphous phase. First, the overall microstructure of the material was controlled by incorporation of a fixed amount of elongated β-Si_3N_4 seeds into the starting powder to regulate the size and fraction of the large reinforcing grains. With controlled microstructures, the interfacial debond strength between the reinforcement and the intergranular glass was optimized by varying the yttria-to-alumina ratio in the sintering additives. It was found that the steady-state fracture toughness value of these silicon nitrides increased with the Y:Al ratio of the oxide additives. The increased toughness was accompanied by a steeply rising *R*-curve and extensive interfacial debonding between the elongated β-Si_3N_4 grains and the intergranular glassy phase. Microstructural analyses indicate that the different fracture behavior is related to the Al (and O) content in the β′-SiAlON growth layer formed on the elongated β-Si_3N_4 grains during densification. The results imply that the interfacial bond strength is a function of the extent of Al and Si bonding with N and O in the adjoining phases with an abrupt structural/chemical interface achieved by reducing the Al concentration in both the intergranular phase and the β′-SiAlON growth layer. Analytical modeling revealed that the residual thermal expansion mismatch stress is not a dominant influence on the interfacial fracture behavior when a distinct β′-SiAlON growth layer forms. It is concluded that the fracture resistance of self-reinforced silicon nitrides can be improved by optimizing the sintering additives employed.

I. Introduction

In silicon nitride ceramics, the presence of a microstructure similar to whisker-reinforced ceramic composites, with elongated β-Si_3N_4 grains as the reinforcing agent, is a necessary but not a sufficient condition to improve the fracture resistance of the material. Silicon nitrides prepared with different densification additives and processing conditions that exhibit self-reinforced microstructures can have very different fracture resistances.[1–4] One of the critical issues in microstructural design of silicon nitride ceramics is to control the debonding behavior at the interface between the β-Si_3N_4 grains and the intergranular glassy phase so that the elongated β-Si_3N_4 grains can contribute to the toughening mechanisms such as crack deflection and crack bridging. Several studies indicated that the interfacial debonding in silicon nitrides could be influenced by the composition of densification additives which ultimately altered the composition of the intergranular amorphous phase.[1–4] However, experimental difficulties exist in systematically investigating the effect of sintering additives on the fracture behavior of silicon nitrides, mainly because different densification additives generally induce different grain growth rates during densification and result in microstructures with different grain morphologies and sizes.

In order to isolate the influence of glass compositions on the debonding behavior at the interface between the elongated β-Si_3N_4 grain and the oxynitride glasses, experiments were conducted with silicon nitride whiskers dispersed in oxynitride glasses with different Y:Al ratios and different rare-earth elements.[5,6] It was found that the interfacial debonding behavior varies with the glass composition. For example, in glasses with high alumina and nitrogen contents, a distinct epitaxial β′-SiAlON layer readily formed on the β-Si_3N_4 whiskers. The whisker/glass interfaces on which a distinct β′-SiAlON interlayer formed exhibited a higher debond strength, as compared to the interfaces where the rise in oxygen (and Al) contents occurred over a very narrow (20–30 nm) interfacial growth region with no visually detected SiAlON layer.[7,8] The observations suggested that in these whisker/glass systems, chemical bonding across the interface determined the strength of the interface while the residual thermal expansion mismatch stress imposed on the interface can modify the debonding length.[6] The next step was to determine the relevance of these observations for optimizing the fracture resistance of silicon nitride ceramics.

Recent success in tailoring the microstructures of silicon nitrides with elongated β-Si_3N_4 seeds presents an ideal material system with which to pursue the study on interfacial debonding and fracture resistance in silicon nitride ceramics. By incorporating a controlled amount of elongated β-Si_3N_4 single-crystal seeds into the ceramics, the seeding method not only provides a novel approach to improve the fracture resistance while retaining high strength,[9,10] but also serves as an effective method to control the microstructure by regulating the size, content, and distribution of the elongated β-Si_3N_4 grains.[9,11] Therefore, the seeded silicon nitride is an ideal material system for investigating the effect of sintering additives on the fracture behavior of silicon nitride ceramics.

This paper, the second of two papers, describes improvements in the fracture resistance of silicon nitride ceramics by microstructural design, emphasizing control of the chemistry of the intergranular glassy phase. The *R*-curve behavior of seeded silicon nitrides densified with different Y:Al ratios is compared and the toughening mechanisms in the materials are investi-

S. M. Wiederhorn—contributing editor

Manuscript No. 190762. Received August 20, 1997; approved February 13, 1998.
Supported by the U.S. Department of Energy, Division of Materials Sciences, Office of Basic Energy Sciences, under Contract No. DE-AC05-960R22464 with Lockheed Martin Energy Research Corp.

*Member, American Ceramic Society.
†Current address: Unilever Research, Bedfordshire, England.

gated by *in situ* observation of crack interaction with microstructural features. The microstructural origin of the different fracture behaviors of these seeded silicon nitrides is addressed.

II. Experimental Procedure

The sintering additives used and the density of the seeded silicon nitride investigated in the present study are listed in Table I. The β-Si_3N_4 seeds were grown by heating a powder mixture of β-Si_3N_4, Y_2O_3, and SiO_2 in a silicon nitride crucible at 1850°C for 2 h under a nitrogen pressure of 0.5 MPa, followed by acid rinse treatments. The final seeds were defect-free rodlike β-Si_3N_4 single-crystal particles with a very low level of impurities (0.26% oxygen and 1.3 ppm yttrium). Details of the preparation and characterization of the seeds are reported in Ref. 12. Seeded silicon nitrides were prepared by tape casting followed by gas pressure sintering. The starting powders were α-Si_3N_4 (E-10 grade, Ube Industries, Japan), Y_2O_3 (purity > 99.9%, BET 27 m^2/g, Hokko Chemicals, Japan), Al_2O_3 (purity > 99.9%, BET 173 m^2/g, Hokko Chemicals, Japan), and 2 vol% β-Si_3N_4 seed particles. The processing procedure is described in detail in Ref. 9. Bulk densities were measured by Archimedes' method and compared with the theoretical density calculated based on phase contents and the bulk densities of β-Si_3N_4 and Si-Al-Y oxynitride glasses.[13,14] As shown in Table I, all of the samples were well densified except those sintered with additives of 6.25 wt% Y_2O_3, and 1.0 wt% Al_2O_3. X-ray diffraction (XRD) analysis was performed to confirm a complete α/β transformation and to identify secondary phases.

Microstructural characterizations of the seeded silicon nitrides were conducted using scanning electron microscopy (SEM) (Model S4100, Hitachi, Tokyo, Japan) equipped with a field emission gun and transmission electron microscopy (TEM) (Model CM200FEG, Philips Electronic Instruments, Mahwah, NJ). For the SEM studies, polished samples were plasma etched using a gas mixture of CF_4 and O_2[15,16] and then carbon coated to prevent electrostatic charging effects. TEM thin foils were prepared in a conventional manner by mechanical grinding, dimpling, argon ion beam milling to perforation, and then carbon coating.

The grain-diameter distribution, the area fraction of large elongated grains, and the glass content in the seeded silicon nitrides densified with different additives were compared by performing quantitative image analyses on digitized SEM photographs. Image analyses were carried out using a commercially available software (PRISM, Analytical Vision, Inc., Raleigh, NC) following the general procedures described in Ref. 17. For grain-size distribution measurement, the magnification of the SEM pictures was optimized so that the whole range of grain sizes was covered and accurate measurements could be obtained. In the present study, three different magnifications (4485×, 7476×, and 37378×) were employed and the diameters of 1500 grains were measured for each composition. To determine the area fraction of large elongated grains, an area of ~1 mm^2 was examined at a magnification of 4485×. For glass content, the images were taken from a polished surface without etching and an area of ~0.25 mm^2 was analyzed at a magnification of 7476×. The orientation of the large elongated grains in compositions A and C was analyzed by manually measuring the angle between the *c*-axis of the large elongated grains and the tape-casting direction; 500 grains were measured in each composition.

Composition analyses were conducted using energy dispersive X-ray spectrometry (EDS) in SEM (Model 400B-1SPT, Noran Instruments, Inc., Middleton, WI) and EDS in TEM (Super UTW, Link/Oxford), both capable of light element detection. For the EDS analyses in SEM, the lateral and depth spatial resolutions were ~100 and ~33 nm, respectively, as determined by a Monte Carlo simulation.[18] The cation concentrations (Al, Si, and Y) were determined from quantification analyses of the EDS spectra and averaged over 3–5 data sets for each area of interest in each composition. EDS spectra collected in SEM were analyzed using the Desk Top Spectrum Analyzer and X-Ray Data Base (DTSA) (National Institute of Standards and Technology, Gaithersburg, MD). EDS spectra collected in TEM were analyzed with background subtraction followed by a standardless quantification routine with absorption correction options.

The *R*-curve response of the seeded silicon nitrides was investigated using an applied moment double cantilever beam (DCB) geometry with the crack plane oriented perpendicular or parallel to the tape-casting direction, along which there was a tendency for the large elongated grains to align. The DCB blanks had dimensions of 10 mm × 35 mm × 2.5 mm. One of the wide surfaces (10 mm × 35 mm) contained a ~1 mm deep by 1.5 mm wide centerline groove parallel to the length while the opposite surface was mechanically polished to facilitate observation of the crack. One end of the specimen was notched and precracked with an initial crack length between 50 and 200 μm. Testing was conducted using an applied moment DCB test module, with load applied through a bending moment on the loading arms attached to the specimens. The testing stage could be placed either under an optical microscope or in the chamber of an SEM (Hitachi S4100) to enable direct observation of the crack interaction with microstructures. Details of the testing module and sample preparation can be found in Refs. 10 and 19.

Flexure strength of the seeded silicon nitrides was measured using a four-point flexure fixture mounted on a universal test machine (Model 1122, Instron), with inner and outer spans of 20 and 40 mm, respectively. The flexure bars had a 4 mm × 3 mm cross section, with the tensile surfaces of the bars parallel to the tape casting surface and the tensile axis parallel to the tape casting direction. Surfaces of the bars were prepared using a 400 grit diamond grinding wheel. Tests were conducted at room temperature in air at ~50% relative humidity and with a loading rate of 70 MPa/s.

III. Results

(1) General Microstructural Characterization

The seeded silicon nitrides exhibited a distinct bimodal microstructure, with large elongated β-Si_3N_4 grains grown from the seed particles embedded in a fine-grain matrix, as evidenced by both a SEM micrograph (Fig. 1(a)) and the grain-

Table I. Sintering Additives Employed, Density, Glass Content, Area Fraction of the Large Elongated Grains, Flexure Strength, and Steady-State Fracture Toughness from *R*-Curve Measurement with Crack Plane Perpendicular ($K_\perp$) or Parallel ($K_\parallel$) to the Casting Direction of the Silicon Nitrides

	Samples		
	A	B	C
Sintering additives (wt%)	$4.0Y_2O_3$:$2.8Al_2O_3$	$5.0Y_2O_3$:$2.0Al_2O_3$	$6.25Y_2O_3$:$1.0Al_2O_3$
Relative density (%)	98	98	94
Glass content (%)	3.7	3.4	4.7
Area fraction of the large elongated grains (%)	29.4	28.7	31.7
Flexure strength (MPa)	1096 ± 48	1011 ± 78	1144 ± 126
$K_\perp$ ($MPa\cdot m^{1/2}$)	7.5 ± 0.2	8.7 ± 0.4	10.6 ± 0.2
$K_\parallel$ ($MPa\cdot m^{1/2}$)	6.9 ± 0.2	7.8 ± 0.3	9.2 ± 0.2

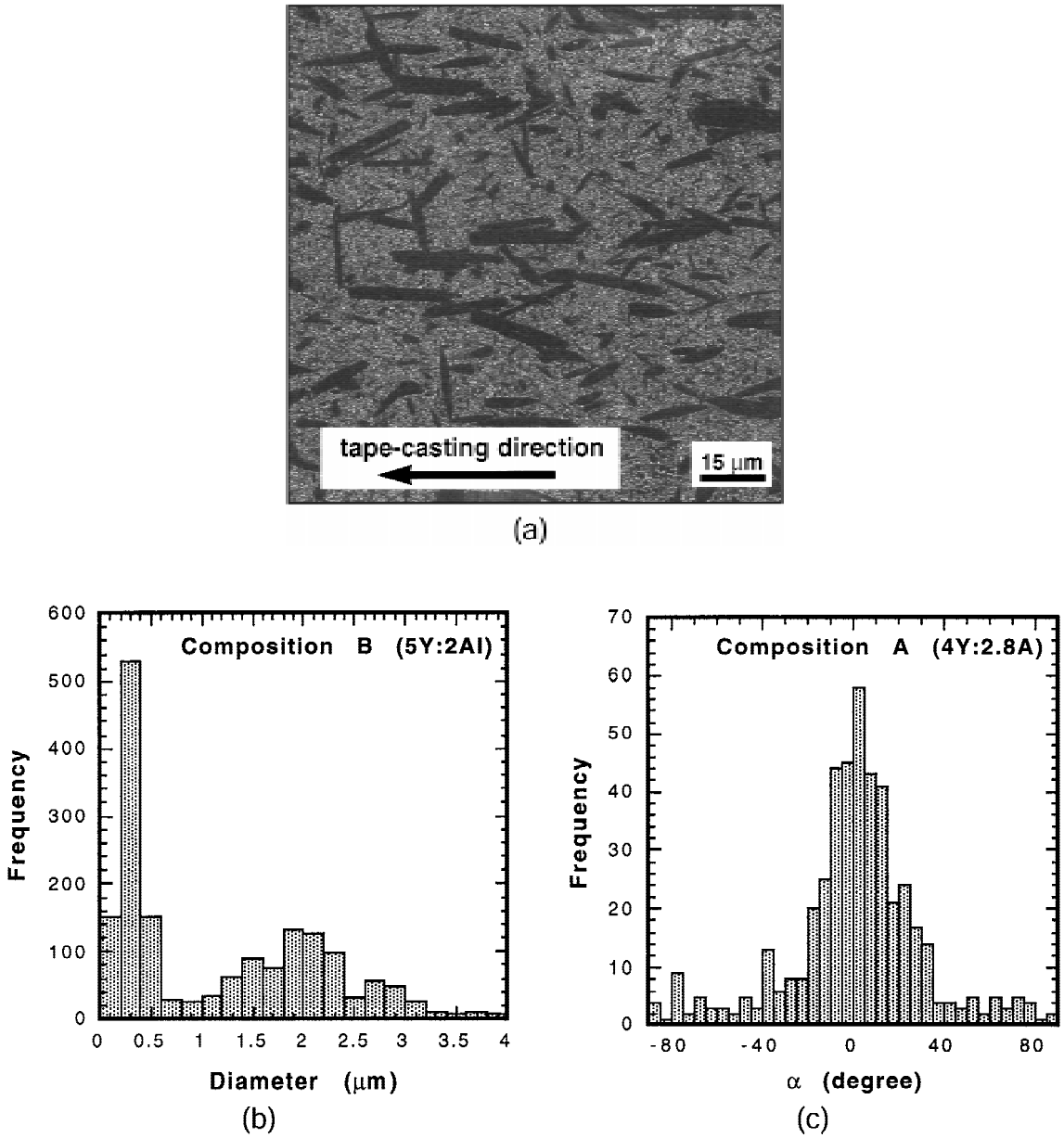

Fig. 1. (a) General microstructures of the seeded silicon nitrides. A bimodal structure was achieved with large elongated grains grown from the seed particles embedded in a fine-grain matrix. (b) Typical grain-size distribution in the seeded silicon nitride (sample B, $5.0Y_2O_3$:$2.0Al_2O_3$). An average of 1500 grains were measured in each composition. (c) Typical orientation-distribution of the large elongated grains along the casting direction (sample A, $4.0Y_2O_3$:$2.8Al_2O_3$). α is the angle between the *c*-axis of the large elongated grains and the casting direction; 500 grains were measured.

size distribution (Fig. 1(b)). Quantitative image analyses indicated that the grain diameters and the diameter distributions were identical in samples with different Y:Al ratios. As shown in Fig. 1(b), the diameter of the fine grains, which composed the matrix in the self-reinforced microstructure, was less than 0.6 μm and most populated at ~0.3 μm. The diameter of the large elongated grains grown from the β-Si_3N_4 seed particles, which functioned as the reinforcing agent in the ceramics, ranged from 1.5 μm to 2.5 μm. The typical aspect ratio of the elongated grains was 6–7. (The seed particles incorporated had an average diameter of ~1 μm and a typical aspect ratio of ~4.[11])

The large elongated β-Si_3N_4 grains in the seeded silicon nitrides tended to lie in the casting planes and to align along the casting direction to a certain degree because of the sheet forming process. The angle between the *c*-axis of the large elongated grains and the casting direction (α) was measured. No variations were observed from compositions A to C, and a typical angle distribution is shown in Fig. 1(c). Because of the small number of seeds incorporated (2 vol%) and the relatively small aspect ratio of the seeds (~4[11]), the large elongated grains were distributed over a conical region along the casting direction instead of unidirectionally (Fig. 1(c)) and the influence of texture on the mechanical properties was not significant (Section III(3)).

Quantitative image analyses showed that the area fraction of the large elongated grains (~29%) and the glass contents (~4%) were similar in all three compositions (Table I). (The slightly higher glass content measured in sample C was partially due to the difficulty during image analyses for the software to distinct pores and the intergranular glass.) Overall, it can be concluded that the microstructures of the seeded silicon nitrides were insensitive to the sintering additives used for densification and the seeding method was effective in regulating the grain morphology, the grain size, and the size distribution in silicon nitride ceramics. Therefore, any difference observed in mechanical properties (fracture resistance and strength), as reported in Section III(3) can be attributed solely to the influence of chemistry induced by the different additive ratios employed.

(2) Composition Analyses

The seeded silicon nitrides prepared in the present study contained only the β-silicon nitride phase, as concluded from the XRD analyses, indicating (1) a complete α/β transformation and (2) an amorphous intergranular phase. Polished and plasma-etched samples were examined using SEM. In all three compositions (A, B, and C), a core/rim structure was always observed in the large elongated grains, as shown in Fig. 2. EDS analyses revealed that the core region contained only Si and N while traces of Al and O were detected in the rim region. The differences in composition influenced the etching rate during the plasma etching process and resulted in the surface features observed in SEM.[15,16] Similar features have been seen in previous studies on grain growth mechanisms in silicon nitrides.[20,21] Structural and chemistry analyses revealed that the core region consisted of β-Si_3N_4 seed particles incorporated in the starting powder and the rim region represented a β′-SiAlON epitaxial growth layer. The fine matrix grains had compositions similar to those of the β′-SiAlON epitaxial growth layer on the large elongated grains.

The chemistry of the β′-$Si_{6-z}Al_zO_zN_{8-z}$ growth layer varied with the sintering additives. Preliminary composition analyses were conducted using EDS in SEM, and typical spectra of each composition are shown in Figs. 3(a–c). The spectra were collected near the center of the β′-$Si_{6-z}Al_zO_zN_{8-z}$ growth region (with equal distances from the end of a large elongated grain and the β′-SiAlON/β-Si_3N_4 interface). Apparently, the Al content in the β′-$Si_{6-z}Al_zO_zN_{8-z}$ phase was fairly low in all three compositions and decreased systematically from sample A to C, consistent with the decreasing Al_2O_3 content employed in the sintering additives. The Al peak was only slightly above the background in sample C with the lowest Al_2O_3 additive content (Fig. 3(c)). (The carbon peaks in all three spectra were from the carbon coating deposited on the samples.) More detailed analyses revealed a compositional gradient in the β′-$Si_{6-z}Al_zO_zN_{8-z}$ growth region. Regular-shaped large elongated grains were chosen and EDS spectra were collected in the β′-SiAlON region, both near the β′-SiAlON/β-Si_3N_4 interface and near the β′-SiAlON/intergranular-glass interface as represented by spots 1 and 2 in Fig. 2. Each spot was located about 200–300 nm away from the corresponding interface. Cation (Si and Al) ratios were calculated from the EDS spectra and are summarized in Table II. In each composition, the Al concentration (the *z* value) decreased from the β′-SiAlON/β-Si_3N_4 interface to the SiAlON/intergranular-glass interface, due to the decreasing amount of Al and O retained in the glassy phase during grain growth. Similar Al gradients have been observed in β′-SiAlON ceramics and have been attributed to the compositional change in the liquid phase during the solution–reprecipitation process.[22,23] In the present seeded silicon nitrides, the Al concentration also decreased systematically from compositions A to C at each location (spots 1 and 2 in Fig. 2). Because of the very

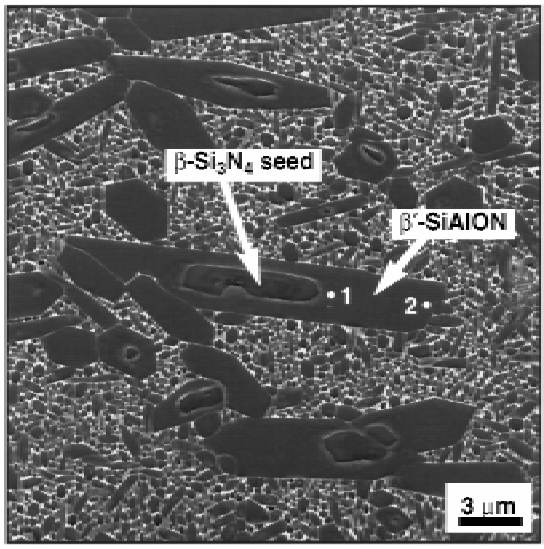

Fig. 2. Core/rim structure observed in the large elongated grains in the seeded silicon nitrides. The core region was the remains of the β-Si_3N_4 seed particles incorporated in the starting powder and the rim region was a β′-SiAlON epitaxial growth layer.

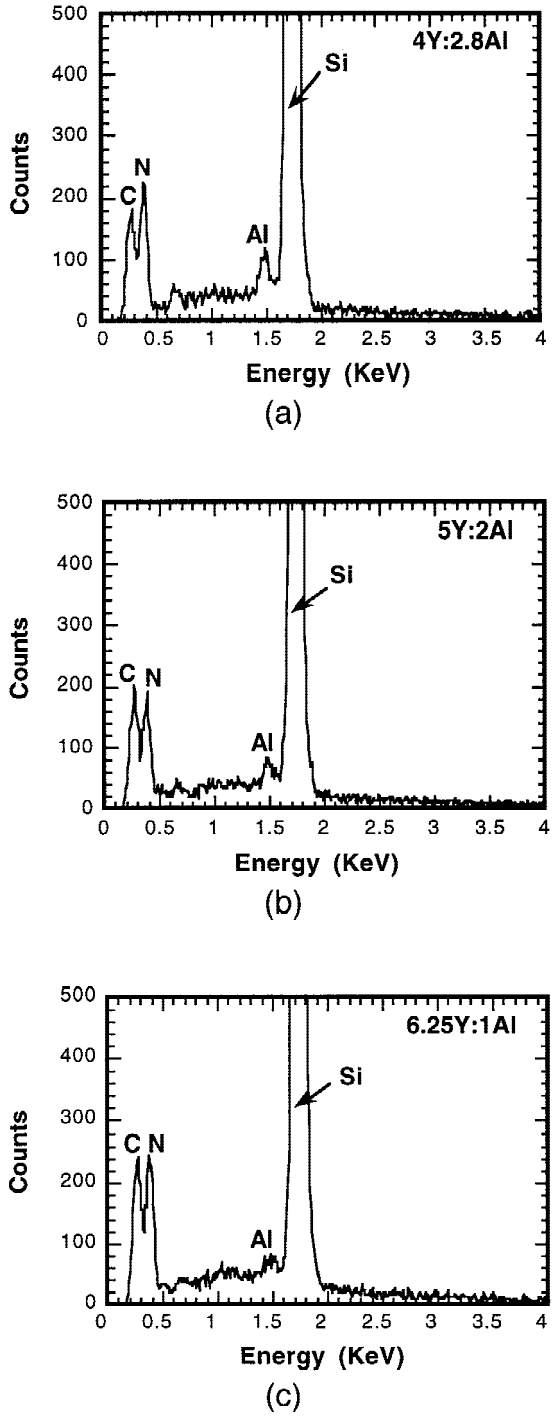

Fig. 3. EDS spectra collected in SEM from the β′-SiAlON layer in the seeded silicon nitrides with different Y:Al ratios: (a) composition A ($4.0Y_2O_3$:$2.8Al_2O_3$), (b) composition B ($5.0Y_2O_3$:$2.0Al_2O_3$), and (c) composition C ($6.25Y_2O_3$:$1.0Al_2O_3$). (The spectra were collected near the center of the SiAlON layer with equal distances from the end of a large elongated grain and the β′-SiAlON/β-Si_3N_4 interface. The carbon peaks in the spectra were from the carbon coating deposited on the samples.)

Table II. Cation Concentrations (Al and Si) and Calculated *z* Values of the β′-$Si_{6-z}Al_zO_zN_{8-z}$ Growth Region in the Three Different Compositions

Samples	Near β′-SiAlON/β-Si_3N_4 interface (SEM)			Near SiAlON/intergranular-glass interface (SEM)			EDS (TEM)
	Al (at.%)	Si (at.%)	*z*	Al (at.%)	Si (at.%)	*z*	*z*
A	0.018	0.982	0.11	0.010	0.990	0.06	0.11
B	0.016	0.984	0.10	0.005	0.995	0.03	
C	0.008	0.992	0.05	0.001	0.999	0.01	0.07

low Al_2O_3 content employed in the composition C sintering additives, the Al concentration (*z* value) approached to near zero at the grain/glass interface.

Previous studies have shown that β′-SiAlON grows epitaxially on β-Si_3N_4.[7,20,24,25] Because of the very low Al and O contents in the β′-$Si_{6-z}Al_zO_zN_{8-z}$ layer in the seeded silicon nitrides ($z \leq 0.11$), the lattice mismatch between the two layers was negligible and hence the core/rim structure and the β′-SiAlON/β-Si_3N_4 interface were generally invisible in TEM thin foils. Average compositions of the β′-$Si_{6-z}Al_zO_zN_{8-z}$ layers were estimated from EDS spectra collected in large grains, with a large probe (~150 nm in diameter) placed ~0.5–1.0 μm from the end of an elongated grain where it should be in the SiAlON region according to Fig. 2 or at the center of a grain oriented along the *c*-axis with a hexagonal cross section. The *z* values calculated from these spectra are ~0.11 and 0.07 for samples A and C, respectively, varying with the same trend as shown by the EDS (SEM) data. Because of the invisibility of the core/rim structure, uncertainty existed about the exact location of the probe in the β′-SiAlON layer and the exact position of the thin TEM foil sectioning the large elongated grains. Comparing the results with EDS (SEM) data (Table II), it appears that the EDS (TEM) spectra may have been collected close to the β′-SiAlON/β-Si_3N_4 interface.

The Y:Al ratios in the sintering additives also influence the composition of the intergranular glass. Figures 4(a) and (b) are typical examples of the EDS spectra collected in TEM from glass pockets at triple grain junctions in samples A and C. The Al concentration decreased while the Y concentration increased steadily from composition A to C. The calculated cation concentrations in the glasses were 55 equiv% Si, 10 equiv% Al, and 35 equiv% Y in sample A, and 52 equiv% Si, 3 equiv% Al, and 45 equiv% Y in sample C. The Y:Al ratios in the intergranular glass in the silicon nitrides (3.5:1 and 15.0:1 for compositions A and C, respectively) are greater than those formulated in the starting powder (2:3 and 3:1 for compositions A and C, respectively, in equiv%), because of the different solubilities of Al and Y in the β-silicon nitride phase. While Al is readily incorporated into the β-Si_3N_4 to form β′-SiAlON, the greater size of Y prevents its incorporation into the β′ lattice structure.

(3) R-Curve Behavior and Fracture Strength

The fracture resistance of the seeded silicon nitrides varied as a function of the Y:Al ratio in the sintering additives. Figure 5 shows the *R*-curves measured for different compositions with the crack plane oriented perpendicular to both the tape-casting plane and the casting direction. Samples A, B, and C all exhibited steeply-rising R-curves; i.e., the fracture resistance of the materials increased rapidly with initial crack extension. The steady-state toughness values, with the crack plane either perpendicular ($K_\perp$) or parallel ($K_\parallel$) to the tape-casting direction, increased systematically with increasing Y:Al ratio in the sintering additives, as summarized in Table I. Composition A with

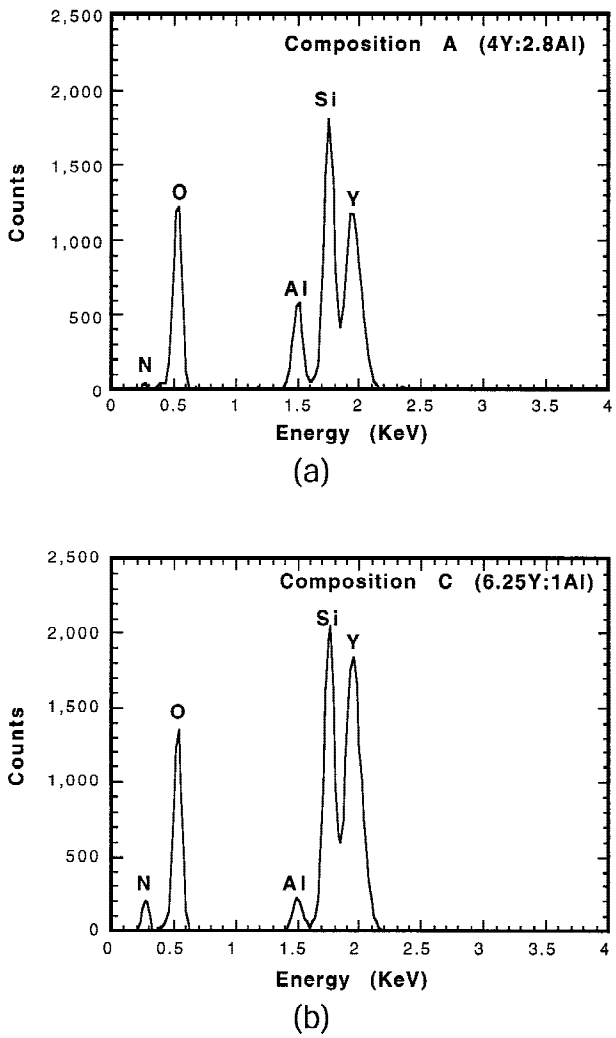

Fig. 4. EDS spectra from glass pockets at triple grain junctions showing that the Al concentration decreased while the Y concentration increased from composition A (a) to C (b).

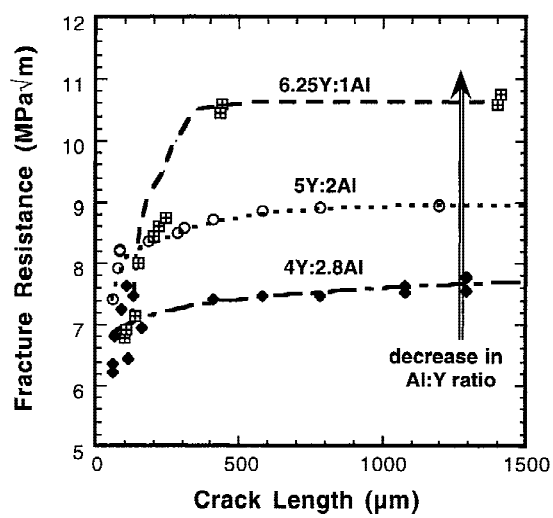

Fig. 5. *R*-curves of seeded silicon nitrides with different compositions. The crack planes were perpendicular to the tape-casting direction.

the lowest Y:Al ratio exhibited a steady-state fracture toughness of ~7.0 MPa·m$^{1/2}$, while composition C with the highest Y:Al ratio exhibited a high fracture toughness value of about 9–11 MPa·m$^{1/2}$. The differences in the steady-state toughness along different orientations were not significantly large because the texture was not strong, as shown in Section III(1).

In situ SEM observation of cracks interacting with the microstructures revealed that the interfacial debonding behavior between the large elongated grains and the intergranular glass varied with the sintering additives employed. As shown in Figs. 6(a) and (b), when the crack approached the reinforcing grains at similar angles of incidence ($\theta \sim 60°$), the large elongated grain in sample A failed transgranularly while crack deflection and interfacial debonding occurred in sample B. When the crack approached the reinforcing grains at smaller angles of incidence (Figs. 6(c) and (d)), interfacial debonding occurred in both samples A and B. However, the debonding lengths were longer in sample B than those in sample A. The critical debonding angles (θ_c), beyond which no crack deflection could occur at the interface, were estimated from *in situ* SEM observations. θ_c values were ~60°, ~70°, and ~75° for compositions A, B, and C, respectively. Apparently, the interface between the large elongated grains and the surrounding glass was more readily to debond and had a lower interfacial debonding energy in samples processed with higher Y_2O_3:Al_2O_3 ratios in the sintering additives. With increasing θ_c, the amount of large elongated grains involved in the toughening process, where the crack intersects at angles smaller than θ_c, should be significantly increased. This is consistent with *in situ* SEM observations that the overall extent of crack deflection and crack bridging which occurred during crack extension increased from compositions A to C with increasing Y:Al ratios. According to previous work on whisker-reinforced ceramic-matrix composites, increases in both the amount of reinforcement and the extent of debonding length result in better fracture resistance.[19]

Unlike ''conventional'' self-reinforced silicon nitride with a coarsened microstructure in which the fracture resistance was improved at the expense of strength, the seeded silicon nitrides investigated here all exhibited exceptionally high flexure strength, as summarized in Table I. The achievement of both

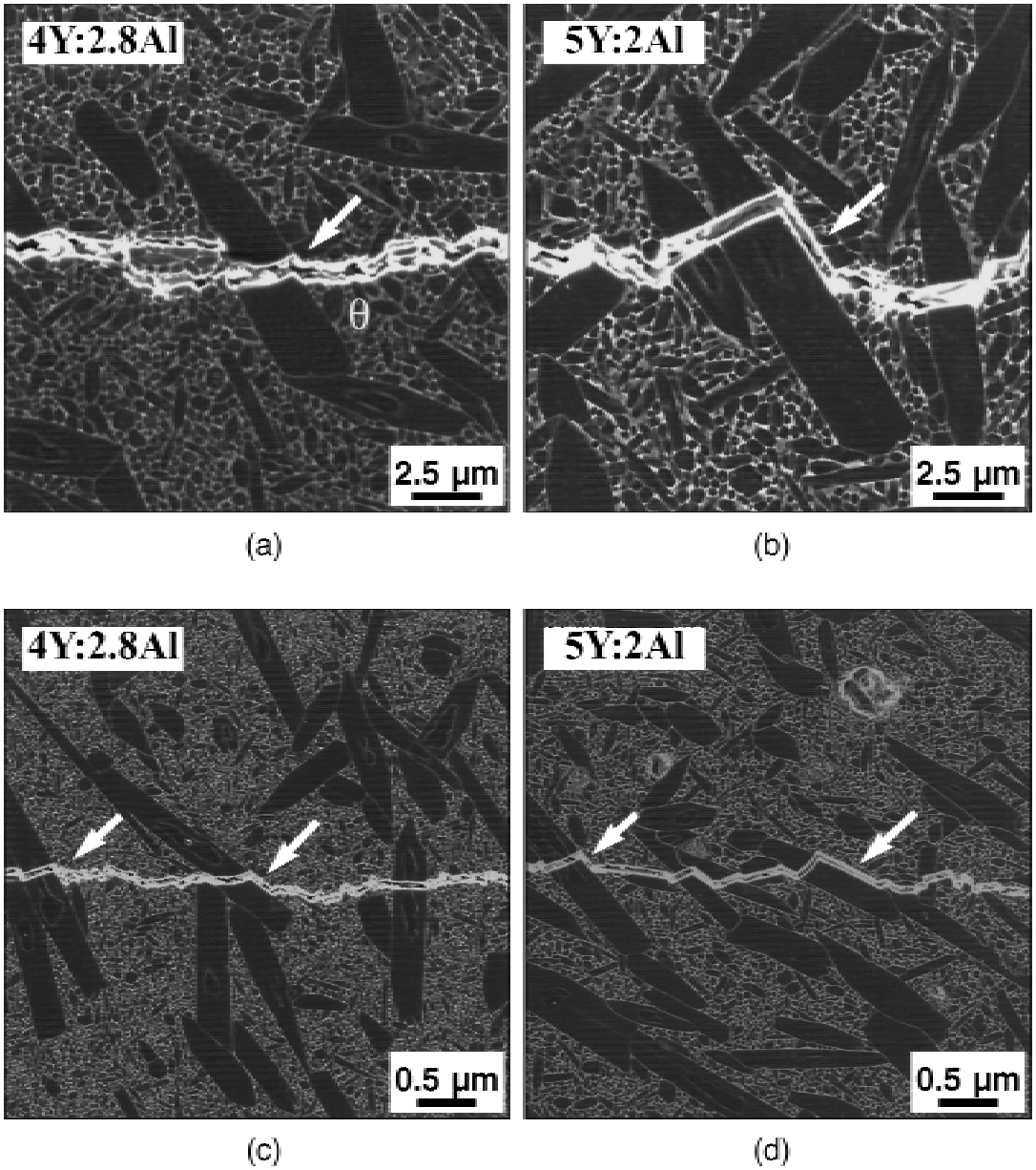

Fig. 6. *In situ* observations of crack interacting with the large elongated grains: the large elongated grain in sample A failed transgranularly (a) while crack deflection and interfacial debonding occurred in sample B (b) when the angles of incidence were large ($\theta \sim 60°$); and sample A exhibited shorter debonding lengths (c) than sample B (d) when the angles of incidence were small and hence debonding occurred in both samples.

high flexure strength and high fracture toughness is attributed to the presence of a bimodal microstructure with large elongated grains well dispersed in a fine-grained matrix, as discussed in detail in the first part of this series.[10]

IV. Discussion

(1) Influence of the Composition of the β′-SiAlON Growth Layer on the Fracture Behavior

The different *R*-curve response of the seeded silicon nitrides indicated that the fracture behavior is strongly influenced by the chemistry near the grain/intergranular-glass interface. This is consistent with observations in previous studies on model systems with silicon nitride whiskers dispersed in oxynitride glasses.[5–8] In the β-Si_3N_4-whisker/Si-Al-Y-oxynitride-glass model systems, interfacial debonding behavior varied with the glass composition. When the Y:Al ratio in the glass was low, a distinct epitaxial β′-SiAlON layer grew on the β-Si_3N_4 grain. Compared to the β-Si_3N_4/oxynitride-glass interface, the β′-SiAlON/oxynitride-glass interface is more resistant to debonding.[5–7] High-resolution analytical electron microscopy revealed that the Al and O concentrations varied more gradually across the β′-SiAlON/oxynitride-glass interface than across the β-Si_3N_4/oxynitride-glass interface where the compositional gradient was confined in a very narrow region (~20 nm wide).[8] The formation of β′-SiAlON represents a change in the nature of the atomic bonding across the interface. Although isostructural with β-Si_3N_4, β′-SiAlON contains Al–N, Al–O, and Si–O bonds in addition to the Si–N bonds. Because the major atomic bonds in the Si-Al-Y oxynitride glasses are Si–O, Si–N, Al–N, and Al–O, similar chemical bonds can be established across the SiAlON/glass interface as well as within the two phases. Thus the SiAlON/glass interface has a potential to be more strongly chemically bonded than the Si_3N_4/glass interface. This concept is schematically illustrated in Fig. 7(a), with arrows representing the ''additional'' bonding sites induced due to the presence of Al and O in the β′-SiAlON lattice.

Continuing this argument, the bonding strength at the β′-SiAlON/Si-Y-Al-oxynitride-glass interface could be influenced by the Al and O concentrations in the β′-SiAlON layer. Increasing Al (and O) contents in the β′-SiAlON growth layer should enhance the continuity of the bonding across the interface. In silicon nitride ceramics, Al and O are incorporated into the β-Si_3N_4 lattice structure during the sintering process. If large β-Si_3N_4 seed particles are incorporated into the starting powder, the β′-SiAlON phase will exist in the ceramics in two forms, one as the growth layer on the large elongated grains and another as the fine matrix grains nucleated during sintering. Because of the limited supply and the ''uniform'' solubility in the β-Si_3N_4 lattice, the Al concentration in the SiAlON layer on the large elongated grains in the seeded silicon nitrides was generally lower than that in the SiAlON growth layer formed on the β-Si_3N_4 whiskers in the whisker/glass model systems. (The whisker/glass model systems contained only 2 vol% β-Si_3N_4 whiskers.) For example, the highest *z* value of the β′-$Si_{6-z}Al_zO_zN_{8-z}$ growth layer among the three compositions in this study was ~0.11 in seeded silicon nitrides of composition A, compared to ~1.0 in the AlY20 whisker/glass model system.[‡,7] Because of the very low Al and O concentrations in the SiAlON layer in the seeded silicon nitrides, very small changes in the amount of Al at the interface could alter the bonding structure significantly, as illustrated in Fig. 7(b), and resulted in different interfacial fracture behavior.

The strong influence of the Al concentration in the SiAlON layer on the interfacial fracture behavior can be elucidated by

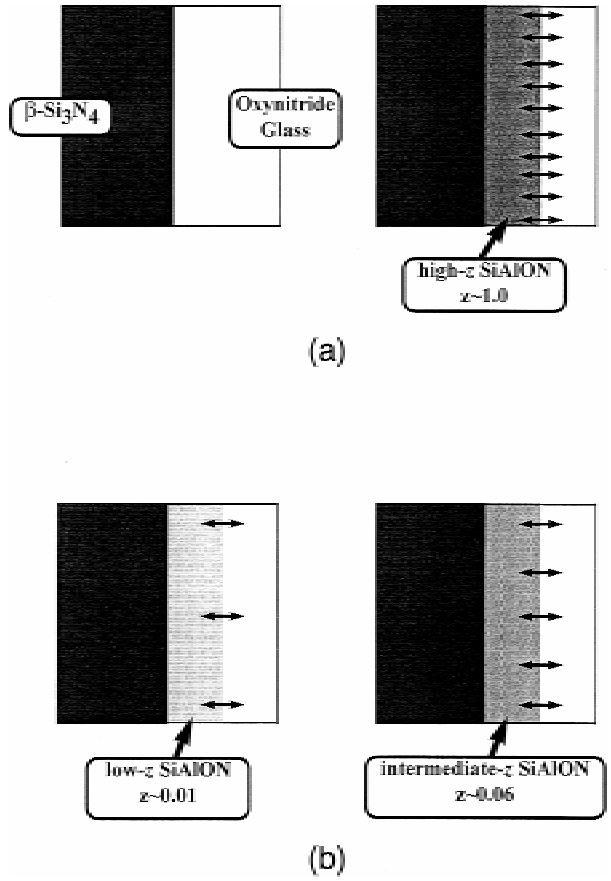

Fig. 7. Schematic diagrams show how the interfacial bond strength between the crystalline phase (β-Si_3N_4 or β′-SiAlON) and the oxynitride glass is influenced by the extent of Al and Si bonding with N and O in the two adjoining phases, with arrows representing the ''additional'' bonding sites induced because of the presence of Al and O in the β-Si_3N_4 lattice structure.

plotting the critical debonding angle (θ_c) versus the *z* value of the SiAlON phase. As shown in Fig. 8(a). data from the whisker/glass model systems (AlY20 and YAl20)[§,5,6] and from the seeded silicon nitrides follow the same trend. The θ_c value decreased most rapidly in the low *z* region (≤ 0.2) and appeared to be approaching an asymptote at high *z* values (≥ 1.0). In the same fashion, the strong influence of the SiAlON composition on the fracture resistance of the seeded silicon nitrides can be shown by plotting the steady-state fracture toughness of the materials versus the *z* value of the SiAlON phase near the β′-SiAlON/intergranular-glass interface listed in Table II (Fig. 8(b)). Evidently, the fracture toughness values are very sensitive to the Al and O concentrations near the grain/glass interface. When the *z* value decreased from 0.06 to 0.01, the toughness value increased by more than 30%.

No significant difference in the interfacial debonding behavior was observed in the previous studies on the whisker/glass model systems with high-Al-content β′-SiAlON growth layers.[6] Perhaps this resulted as the interfacial debonding strength appeared to reach a constant value when the *z* value in the SiAlON layer rose above a certain level, as suggested in Fig. 8(a). (The Al concentrations in the β′-$Si_{6-z}Al_zO_zN_{8-z}$ layers in the model systems were much higher than those formed in the seeded silicon nitride, with *z* values ≥ 1.0.[5,7]) Ongoing and future research is being and will be carried out, in both high-

‡In the AlY20 system, 2 vol% β-Si_3N_4 whiskers were incorporated into an oxynitride glass. The composition of the glass was 55 equiv% Si, 25 equiv% Al, 20 equiv% Y, 80 equiv% 0, and 20 equiv% N.

§The glass composition in YAl20 was 55 equiv% Si, 10 equiv% Al, 35 equiv% Y, 80 equiv% O, and 20 equiv% N.

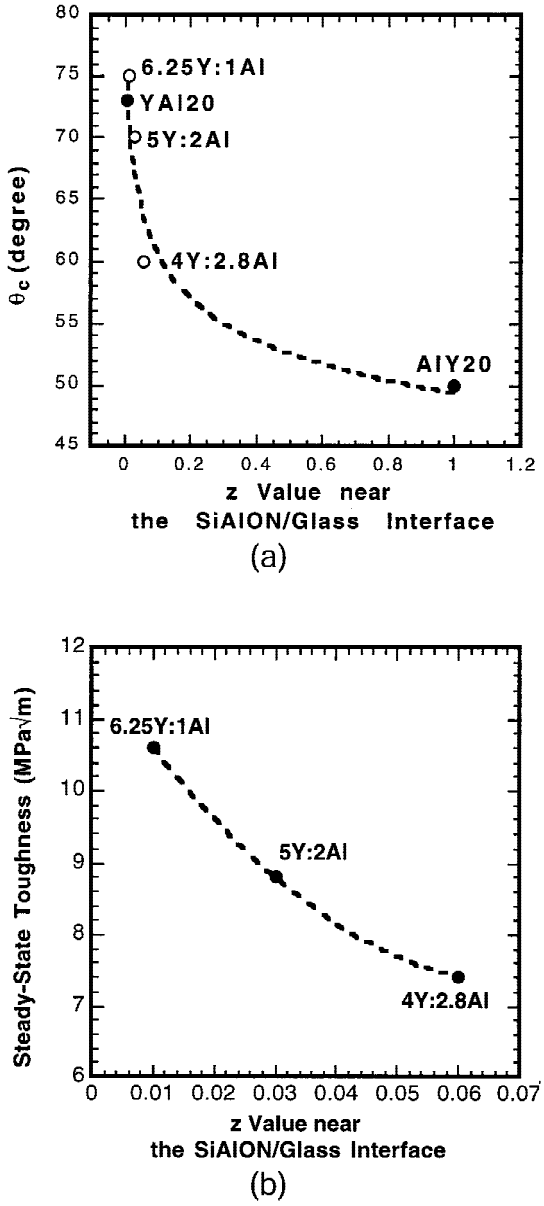

Fig. 8. (a) The critical debonding angle (θ_c) of the SiAlON/glass interface varied as a function of the *z* value of the SiAlON phase (open symbols are data from the seeded silicon nitrides and the filled symbols are data from the whisker/glass model systems[5,6]); and (b) the steady-state fracture toughness of the materials varied as a function of the *z* value of the SiAlON phase near the β′-SiAlON/intergranular-glass interface.

resolution analytical microscopy and analytical modeling, to study the structure and chemistry of both the β-Si_3N_4/oxynitride-glass interfaces and the β′-SiAlON/oxynitride-glass interface at an atomic scale[8,26] and to calculate the interfacial bonding strengths associated with these interfaces.

It should be pointed out that the Al content (the *z* value) in the β′-SiAlON growth layer varies not only as a function of the sintering additives employed but also as a function of the extent of grain growth. As shown in Section III(2) (Table II), the Al concentration (the *z* value) decreased from the β′-SiAlON/β-Si_3N_4 interface to the SiAlON/intergranular-glass interface because of the decreasing amount of Al and O retained in the glassy phase during grain growth. Processing conditions such as the temperatures employed and the holding time at temperatures can indirectly influence the interfacial chemistry by controlling the grain growth process. This finding has two implications. First, it is not necessary to eliminate the addition of Al_2O_3 in order to obtain tough silicon nitrides. Small amounts of Al_2O_3 (~1 wt%) still can be used to facilitate the densification process. Even though SiAlON growth will occur because of the presence of alumina, the Al concentration at the grain/glass interface will be low enough to promote interfacial debonding because of grain growth, as demonstrated in the seeded silicon nitride sample C. Second, simple comparisons of the effects of the initial additive composition is only valid when the silicon nitrides exhibit similar grain morphologies, sizes, and size distributions. It will be necessary to conduct detailed interfacial compositional characterization on individual samples if the materials experienced different processing conditions and exhibited different grain morphologies and size distributions in order to determine effects of interfacial characteristics on the fracture resistance response.

(2) Influence of Thermal Expansion Mismatch Stresses on the Fracture Behavior

It has been suggested that the interfacial debonding behavior and hence the fracture toughness can be influenced by residual thermal expansion mismatch stresses in silicon nitride.[27] As shown earlier, the pertinent thermomechanical properties of the oxynitride glass are, indeed, functions of the glass composition.[14,28] Therefore, analyses of residual stresses imposed on the interfaces were conducted to ascertain their impact on the behavior observed in the present materials. Previously, only the hydrostatic residual stresses in the silicon nitride grains and in the grain boundary phase were calculated using a modified Eshelby model.[27] In the present study, a model of an elongated grain surrounded by a glass film and embedded in a matrix (Fig. 9(a)) was used to simulate the microstructure of the seeded silicon nitrides. This allowed the pertinent radial (and axial) residual stresses action on the interfaces to be examined. The elongated grain was assumed to be single-crystal β-Si_3N_4. Two glass compositions were used to approximate the intergranular glass in seeded silicon nitrides: 56 equiv% Si, 12 equiv% Al, 32 equiv% Y, 83 equiv% O, and 17 equiv% N for composition A (abbreviated as glass A in Table III); and 56 equiv% Si, 4 equiv% Al, 40 equiv% Y, 83 equiv% O, and 17 equiv% N for composition C (glass C). These two glass compositions were chosen because (1) the cation ratios are close to those in the seeded silicon nitrides A and C, as determined by EDS analyses (Section III(2)); and (2) the thermal/mechanical properties have been systematically studied in a previous report.[14] The matrix was assumed to be a mixture of fine-grain β-Si_3N_4 (90 vol%) and the corresponding oxynitride glass (10 vol%). A simple ''rule-of-mixtures'' approach was used to calculate the properties of this ''matrix.'' Table III lists the values of the elastic modulus (*E*), the Poisson ratio (ν), the thermal expansion coefficient (α), and the glass transition

Table III. Properties of the Crystalline Phase and the Si-Al-Y Oxynitride Glasses for Residual Stress Analyses

	E (GPa)	ν	α ($\times 10^{-6}$/°C)	T_g (°C)
β-Si_3N_4	320 (Ref. 29)	0.26	2.01 (*a*-axis, Ref. 29) 2.84 (*c*-axis, Ref. 29)	
Glass A (Ref. 14)	142	0.29	6.4	959
Glass C (Ref. 14)	144	0.29	7.2	986

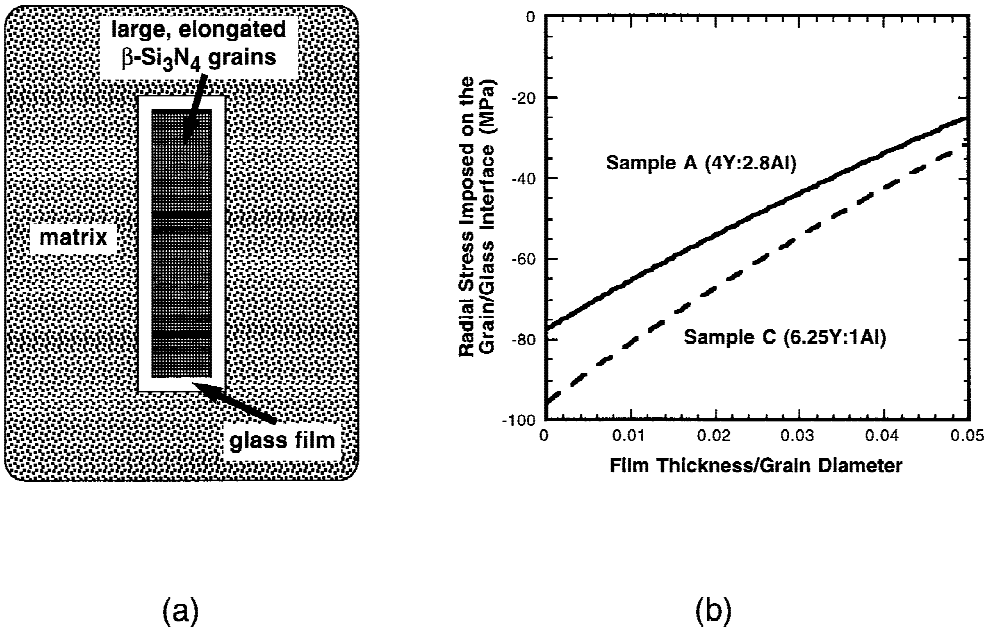

Fig. 9. (a) Model used to simulate the microstructure of the seeded silicon nitride—an elongated grain surrounded by a thin film of glass and embedded in a matrix. The matrix is treated as a mixture of silicon nitride grains and the oxynitride glass. (b) Calculated radial residual stress imposed on the grain/glass interface as a function of the glass film thickness. The compressive stress at the interface increases slightly with increasing Y:Al ratios.

temperature (T_g) used here. Note that although a SiAlON phase formed during sintering, no distinction was made in the analyses between β′-SiAlON and β-Si_3N_4 because the difference in thermal/mechanical properties between the two phases is insignificant at very low Al contents ($z < 0.5$).[29]

Thermal expansion mismatch stresses in a whisker-reinforced composite structure have been analyzed using modified Eshelby models, in which whiskers are simulated as ellipsoidal inclusions.[30,31] However, the modified Eshelby model can analyze only two-component systems. In order to incorporate an interfacial layer between the inclusion and matrix and to analyze the stress component at the interface, the system shown in Fig. 9(a) was further simplified to a cylindrical elongated β-Si_3N_4 grain surrounded by a glass film and embedded in a matrix. This simplification is employed because the typical aspect ratio of the large elongated grains in the seeded silicon nitride is 6–7. According to the modified Eshelby model, in a system with ellipsoidal β-Si_3N_4 crystals embedded in an oxynitride glass, the interfacial stress values are insensitive to the length of the inclusions when the aspect ratio is larger than 5.[31] Details of the residual-stress analyses in a cylindrical geometry can be found in Ref. 32. Figure 9(b) illustrates the radial stress imposed on the interface between the large elongated grain and the glass film as a function of the glass-film thickness. In seeded silicon nitrides, the thickness of the glass film varied from several angstroms for grain boundary films to ~100 nm for the triple-junction pockets and the average diameter of the large elongated grains was ~2.0 μm. Within this range of interests (film thickness/grain diameter ratio ≤0.05:1), the interface between the large elongated grain and the glass film is subjected to radial compressive stresses. The magnitude of the stress increases with increasing Y:Al ratios, suggesting that the interfacial debonding would be more difficult in composition C, which is in contrast to the experimental observations. Also, the difference in the thermal expansion mismatch stresses between the two systems is relatively small and is not expected to affect the interfacial fracture behavior significantly. Therefore, as with the Si_3N_4-whisker/oxynitride-glass model systems,[5] the thermal expansion mismatch stress is not a dominant influence on the interfacial fracture behavior in the seeded silicon nitride ceramics, at least when a distinct β′-SiAlON growth layer forms.

V. Conclusion

The microstructure and fracture behavior of silicon nitrides with large elongated seeds were characterized. It was found that the seeding method was effective in regulating the microstructures such as the fraction and the size distribution of the reinforcing agents. With a well-controlled microstructure, the fracture resistance of silicon nitride was systematically studied as a function of the intergranular chemistry. Significant improvement in the *R*-curve behavior and the steady-state fracture toughness values was observed in seeded silicon nitride processed with a high Y:Al ratio in the sintering additives. Compared to silicon nitrides with low Y:Al ratios, the high Y:Al ratio materials exhibited more extensive debonding at grain boundary interfaces, resulting in increased intergranular fracture. Microstructural and chemistry characterization revealed that the Y:Al ratios in the additives influence the atomic bonding structure across the β-Si_3N_4/intergranular-glass interface by altering the composition of the glassy phase and inducing different Al and O contents in the growth region of the elongated grains. Analytical modeling indicated that the thermal expansion mismatch stress has no significant influence on the fracture behavior when distinct β′-SiAlON growth occurs in the materials. It is concluded that reducing the Al concentration in the ceramics could result in a more abrupt structural/chemical interface and ultimately achieve improved fracture resistance by activation of toughening mechanisms such as crack-deflection and crack-bridging via interfacial debonding.

Acknowledgments: We thank Dr. S. X. Ren for calculating the spatial resolution of the EDS(SEM) analyses, and Drs. M. K. Ferber and S. D. Nunn for reviewing the manuscript. Support for K.P.P. in the form of a MITI International Science and Technology Fellowship to conduct processing studies at NIRI–Nagoya is gratefully acknowledged.

References

[1]Y. Tajima, K. Urashima, M. Watanabe, and Y. Matsuo, ''Fracture Toughness and Microstructure Evaluation of Silicon Nitride Ceramics''; pp. 1034–41

in Ceramic Transactions, Vol. 1, *Ceramic Powder Science–IIB.* Edited by G. L. Messing, E. R. Fuller, Jr., and H. Hausner. American Ceramic Society, Westerville, OH, 1988.

[2]Y. Tajima, ''Development of High-Performance Silicon Nitride Ceramics and Their Application,'' *Mater. Res. Soc. Symp. Proc.*, **287**, 189–96 (1993).

[3]K. Urashima, Y. Tajima, and M. Watanabe; p. 235 in *Fracture Mechanics of Ceramics*, Vol. 9. Edited by R. C. Bradt. Plenum Press, New York, 1992.

[4]G. Wötting and G. Ziegler, ''Influence of Powder Properties and Processing Conditions on Microstructure and Mechanical Properties of Sintered Si_3N_4,'' *Ceram. Int.*, **10** [1] 18–22 (1984).

[5]P. F. Becher, E. Y. Sun, C. H. Hsueh, K. B. Alexander, S. L. Hwang, S. B. Waters, and C. G. Westmoreland, ''Debonding of Interfaces Between Beta-Silicon Nitride Whiskers and Si-Al-Y Oxynitride Glasses,'' *Acta Mater.*, **44**, 3881 (1996).

[6]E. Y. Sun, P. F. Becher, S. B. Waters, C. H. Hsueh, K. P. Plucknett, and M. J. Hoffmann, ''Control of Interface Fracture in Silicon Nitride Ceramics: Influence of Different Rare Earth Elements''; pp. 779–86 in *Ceramic Microstructures '96: Control at the Atomic Level.* Edited by A. P. Tomsia and A. Glaser. Plenum Press, New York, 1998.

[7]E. Y. Sun, K. B. Alexander, P. F. Becher, and S. L. Hwang, ''β-Si_3N_4 Whiskers Embedded in Oxynitride Glasses: Interfacial Microstructure,'' *J. Am. Ceram. Soc.*, **79** [10] 2626–32 (1996).

[8]K. B. Alexander, P. Rice, I. M. Anderson, P. F. Becher, and E. Y. Sun, ''Characterization of Interfacial Chemistry and Bonding in Silicon Nitride-Base Ceramics''; presented at the 99th Annual Meeting of the American Ceramic Society, Cincinnati, OH, May 7, 1997 (Nanotechnology Symposium, Paper No. B-078-97).

[9]K. Hirao, M. Ohashi, M. E. Brito, and S. Kanzaki, ''Processing Strategy for Producing Highly Anisotropic Silicon Nitride,'' *J. Am. Ceram. Soc.*, **78**, 1687–90 (1995).

[10]P. F. Becher, E. Y. Sun, K. P. Plucknett, K. B. Alexander, C. H. Hsueh, H. T. Lin, S. B. Waters, and C. G. Westmoreland, ''Microstructural Design of Silicon Nitride with Improved Fracture Toughness: I, Effects of Grain Shape and Size,'' *J. Am. Ceram. Soc.*, **81** [12] 000–000 (1998).

[11]K. Hirao, T. Nagaoka, M. E. Brito, and S. Kanzaki, ''Microstructure Control of Silicon Nitride by Seeding with Rodlike β-Silicon Nitride Particles,'' *J. Am. Ceram. Soc.*, **77**, 1857–62 (1994).

[12]K. Hirao, A. Tsuge, M. E. Brito, and S. Kanzaki, ''Preparation of Rodlike β-Si_3N_4 Single Crystal Particles,'' *J. Am. Ceram. Soc. Jpn.*, **101**, 1051–52 (1993).

[13]T. Rouxel, ''Rheological Behavior of YSiAlON Glasses—Its Incidence on the High-Temperature Deformation of Si_3N_4 Ceramics Sintered with Al_2O_3 and Y_2O_3 Additives''; pp. 175–86 in *Tailoring of Mechanical Properties of Si_3N_4 Ceramics.* Edited by M. J. Hoffmann and G. Petzow. Kluwer Academic Publishers, Dordrecht, Netherlands, 1994.

[14]H. Lemercier, T. Rouxel, D. Fargeot, and J. L. Besson, ''Yttrium SiAlON Glasses: Structure and Mechanical Properties—Elasticity and Viscosity,'' *J. Non-Cryst. Solids*, **201**, 128–45 (1996).

[15]C. Chatfield and H. Norstrom, ''Plasma Etching of SiAlON,'' *J. Am. Ceram. Soc.*, **66** [9] C-168 (1983).

[16]U. Taffner, M. J. Hoffmann, and M. Krämer, ''A Comparison of Different Physical-Chemical Methods of Etching for Silicon Nitride Ceramics,'' *Pract. Metallogr.*, **27**, 385 (1990).

[17]J. C. Russ, *The Image Processing Handbook*, 2nd ed. CRC Press, Ann Arbor, MI, 1994.

[18]S. X. Ren, E. A. Kenik, and K. B. Alexander, ''Exploring Spatial Resolution in EBSD Experiments via Monte Carlo Simulation,'' *Microanal.*, **4** [2] (1998).

[19]P. F. Becher, C. H. Hsueh, K. B. Alexander, and E. Y. Sun, ''Influence of Reinforcement Content and Diameter on the *R*-Curve Response in SiC-Whisker-Reinforced Alumina,'' *J. Am. Ceram. Soc.*, **79**, 298–304 (1995).

[20]M. Kramer, M. J. Hoffmann, and G. Petzow, ''Grain Growth Studies of Silicon Nitride Dispersed in an Oxynitride Glass,'' *J. Am. Ceram. Soc.*, **76** [11] 2778–84 (1993).

[21]M. Kramer, M. J. Hoffmann, and G. Petzow, ''Grain Growth Kinetics of Si_3N_4 during α/β-Transformation,'' *Acta Mater.*, **41** [10] 2939–47 (1993).

[22]D. A. Bonnell, M. Rühle, and T. Y. Tien, ''Redistribution of Aluminum Ions During Processing of SiAlON Ceramics,'' *J. Am. Ceram. Soc.*, **69** [8] 623–27 (1986).

[23]N. K. Kim, D. Y. Kim, A. Kranzmann, E. Bischoff, and S. L. Kang, ''Variation of Aluminum Concentration in β′-SiAlON Grains Formed during Liquid-Phase Sintering of Si_3N_4–Al_2O_3–Nd_2O_3,'' *J. Mater. Sci.*, **28**, 4355–58 (1993).

[24]N. Mirosaki, M. Tanimura, Y. Okamoto, Y. Akimune, and M. Mitomo, ''TEM Analysis of Core/Rim Structure in Silicon Nitride Ceramics,'' *J. Am. Ceram. Soc. Jpn.*, **102**, 873–77 (1994).

[25]K. Rajan and P. Sajgalik, ''Crystallization Induced Sub-Grain Boundaries in Silicon Nitride''; pp. 213–28 in *Engineering Ceramics 96: Higher Reliability through Processing.* Edited by G. N. Babini, M. Haviar, and P. Sajgalik. Kluwer Academic Publishers, Dordrecht, Netherlands, 1997.

[26]P. M. Rice, K. B. Alexander, and I. M. Anderson, ''Multivariate Statistical Analysis of Spectrum Lines from Si_3N_4 Grain Boundaries''; pp. 945–46 in *Proc. Microsc. Microanal., 1997.* Edited by G. W. Bailey, R. V. W. Dimlich, K. B. Alexander, J. J. McCarthy, and T. P. Pretlow. Springer-Verlag, New York, 1997.

[27]I. M. Peterson and T. Y. Tien, ''Effect of the Grain Boundary Thermal Expansion Coefficient on the Fracture Toughness in Silicon Nitride,'' *J. Am. Ceram. Soc.*, **78** [9] 2345–52 (1995).

[28]E. Y. Sun, P. F. Becher, S. L. Hwang, S. B. Waters, G. M. Pharr, and T. Y. Tsui, ''Properties of Silicon–Aluminum–Yttrium Oxynitride Glasses,'' *J. Non-Cryst. Solids.*, **208**, 162–69 (1996).

[29]I. Tanaka, S. Nasu, H. Adachi, Y. Miyamoto, and K. Niihara, ''Electronic Structure behind the Mechanical Properties of β-SiAlONs,'' *Acta Mater.*, **40** [8] 1995–2001 (1992).

[30]Z. Li and R. C. Bradt, ''Micromechanical Stresses in SiC-Reinforced Al_2O_3 Composites,'' *J. Am. Ceram. Soc.*, **72** [1] 70–77 (1989).

[31]C. H. Hsueh and P. F. Becher, ''Residual Thermal Stresses in Ceramic Composites, Part I: with Ellipsoidal Inclusions,'' *Mater. Sci. Eng.*, **A212**, 22–28 (1996).

[32]C. H. Hsueh, P. F. Becher, and P. Angelini, ''Effects of Interfacial Films on Thermal Stresses in Whisker-Reinforced Ceramics,'' *J. Am. Ceram. Soc.*, **71** [11] 929–21 (1988). □